AD-A080 214 AIR FORCE INST OF TECH WRIGHT-PATTERSON AFB OH SCHOO--ETC F/G 20/14
VALIDATION AND RECEIVER DESIGN FOR A RANDOM POINT PROCESS MODEL--ETC(U)
DEC 79 J F STACH
UNCLASSIFIED AFIT/GE/EE/79-34 NL

END
DATE FILMED
3 - 80
DDC

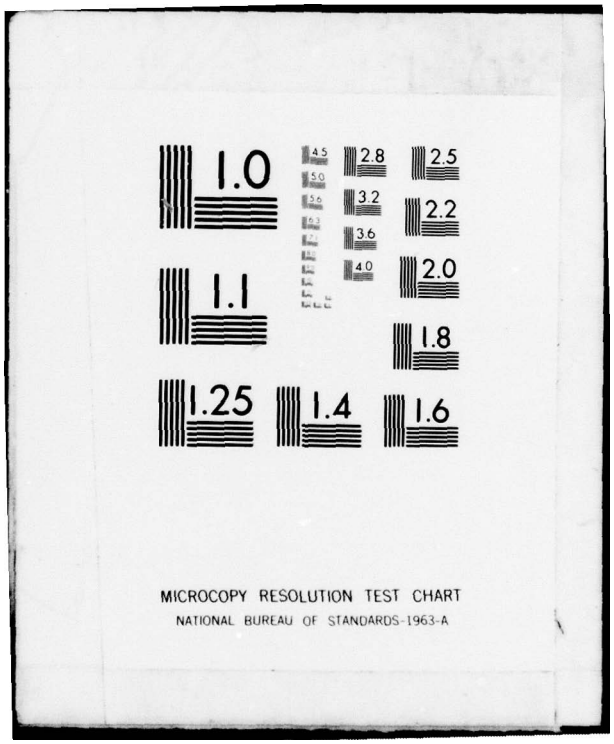
1.0
1.1
1.25
1.4
1.6
1.8
2.0
2.2
2.5
2.8
3.2
3.6
4.0
4.5
5.0
5.6
MICROCOPY RESOLUTION TEST CHART
NATIONAL BUREAU OF STANDARDS-1963-A

LEVEL II

UNITED STATES AIR FORCE
AIR UNIVERSITY

AIR FORCE INSTITUTE OF TECHNOLOGY

Wright-Patterson Air Force Base, Ohio

AFIT/GE/EE/79-34

VALIDATION AND RECEIVER DESIGN FOR A RANDOM POINT PROCESS MODEL OF ATMOSPHERIC RADIO NOISE

THESIS

AFIT/GE/EE/79-34

John F. Stach
2nd Lt USAF

(14) AFIT/GE/EE/79-34

(12) 65

(6) VALIDATION AND RECEIVER DESIGN FOR A RANDOM POINT PROCESS MODEL OF ATMOSPHERIC RADIO NOISE.

(9) Master's THESIS,

Presented to the Faculty of the School of Engineering of

The Air Force Institute of Technology

Air University

In Partial Fulfillment of the Requirements for the

Degree of Master of Science

By

(10) John F. Stach, B.S.
2nd Lt USAF

Graduate Electrical Engineering

(11) December 1979

Approved for public release; distribution unlimited

012225

Preface

This thesis is a closer look at an atmospheric radio noise (ARN) model proposed by Steven Hettinger, a former AFIT student. Hettinger found that the existing models of ARN are not tractable through existing receiver structure and that higher order statistics are not available for these models. The proposed model is simple enough to be tractable and yet complex enough to model many types of ARN. In this report, the statistics of the model are derived, an optimal receiver for communication through this noise is computed, and the accuracy of the model is examined by comparing the first order statistics of the model to measured first order statistics.

I would like to thank my advisor, Major Joseph Carl for his support and guidance throughout this research. I would also like to thank Captain Stanley Robinson for his advice in many areas and Captain Pedro Rustan for his aid in understanding the nature of lightning. I must also give special thanks to my wife Rosann for her support throughout the project.

John F. Stach

Contents

List of Figures

List of Tables

Abstract

An investigation of low frequency atmospheric radio noise (ARN) indicates that the return stroke from lightning discharges is the major source of the noise. A model of ARN is then presented which is based on the return stroke.

The model consists of the sum of two marked Poisson processes. The sum of marked Poisson processes can be thought of as a single marked Poisson process with a transformed rate and a mixture density on the marks. The complete statistical description of this process is then derived and a minimum probability of error processor is designed using the ARN model as the noise.

The theoretical amplitude probability distribution (APD) is then derived for the output of a quadrature envelope detector using the ARN model as an input. The theoretical APD curves were then compared to a measured APD curve from CCIR report 322 and two measured APD curves from an article by K. Furutsu and T. Ishida. The linear mean square error (MSE) between the theoretical and measured curves when plotted on Rayleigh paper is .018 and .015 for the Furutsu and Ishida data, and .018 for the CCIR data.

Based on the first order statistics, the model is found to be a good representation of low frequency ARN. It is therefore recommended that the model be used to evaluate receiver performance in the low frequency channel and that a more thorough validation study be done including a validation of higher order statistics.

VALIDATION AND RECEIVER DESIGN FOR A RANDOM POINT PROCESS MODEL OF ATMOSPHERIC RADIO NOISE

I. Introduction

The increasing demand for communications has created an increasing demand for usable frequency bands. The low frequency spectrum (D.C. to 30 MHz) is usable, but it has a type of noise that is different than in the high frequency spectrum. In the low frequency channel, atmospheric noise is frequently the limiting factor on the performance of communication systems (Ref 15). It is necessary to know detailed statistics of the noise in order to calculate the channel capacity or error rate of a noisy channel. Also, receiver performance can be analyzed if a model with accurate statistics can be traced through a mathematical representation of the receiver. Finally, an accurate model for which the complete statistics are known will allow an optimal Bayes receiver to be designed for the channel. In this report, a model of low frequency atmospheric noise (ARN) is examined. The purposes of this report are to (1) determine the validity of the model, (2) to determine the possibility of using the model to compute the performance of low frequency receivers and (3) to determine the possibility of designing optimal receivers for the low frequency channel.

This report will be divided into four major sections. (1) First, the causes of ARN are examined. The main source of low frequency ARN is found to be the return stroke of cloud to ground lightning discharges. (2) Then, a sum of marked Poisson processes is used to model the ARN. It is found that the resulting process can be written in terms of a single Poisson process with a mixture density on the marks. The minimum probability of error processor is then derived. (3) A validation study is then done to determine the accuracy of the model. Measured amplitude probability distributions (APD) of the output of an envelope detector are then compared to the theoretical APD curves of the model. The measured APD curves are taken from CCIR Report 322 (Ref 22) and an article written by Furutsu and Ishida from Japan (Ref 3). The mean square error between theoretical and measured APD curves plotted on Rayleigh paper is found to be .018 and .015 for two typical curves from the Furutsu and Ishida article, and .018 for a typical curve from CCIR Report 322. (4) Finally, some conclusions about the model will be made along with the recommendations that the model be more thoroughly validated and that the model be used for perfor-mance analysis of receivers for the low frequency channel.

The next section describes the physical processes involved in ARN and some of the properties of ARN that will affect the parameters of an ARN model.

II. Background

There are several types of noise than can interfere with low frequency communications. In the low frequency spectrum, man-made, galactic, and atmospheric noise are the typical types. Man-made noise comes from power lines, machinery, or transmitters. Propagation of man-made noise other than transmitters is principally through power lines and by ground wave (Ref 22:9). Galactic noise power figures are available, and can also influence low frequency noise depending on the frequency and directional properties of the antenna (Ref 22:11). It is important to mention man-made and galactic noise because of the situational factors that could allow these types of noise to dominate a received waveform. However, the articles used to verify the model to be presented attempt to isolate the atmospheric noise and assume that the atmospheric noise predominates at the frequencies of interest (Refs 3, 22). Because of this, the model is designed to represent only the atmospheric noise.

At any given time, there are many lightning storms around the world. The total electromagnetic radiation that reaches a receiver from these storms will be referred to as atmospheric noise. Lightning is the main source of atmospheric noise. Lightning can be defined as a transient, high current discharge. Lightning occurs when some region of the atmosphere attains an electric charge sufficiently large that the electric fields due to the charge cause electrical breakdown

of the air. Uman (Ref 16) treats the subject of lightning thoroughly in his book which is used as a reference in the following discussion. Lightning can occur within a cloud (cloud discharges), between two clouds (cloud to cloud discharges), between a cloud and the earth (ground discharges), or between a cloud and the surrounding air (air discharges). The type most people are familiar with are ground discharges. A total ground discharge is called a flash. A ground flash is composed of one or more separate strokes in the same or separate ionized paths. Each stroke lasts for milliseconds and the time interval between strokes is roughly 50 msec. The flash begins when the regions between some of the positive and negatively charged areas of a cloud achieve a potential greater than the ionization potential. A cloud potential stepped leader then moves toward the ground in roughly 50 m steps with a pause time of about 50 usec between each step. Several branches may propogate toward the ground until one or more brings cloud potential near enough to the ground for a return stroke to occur. When the stepped leader gets near the ground, the resulting field causes a column of ground potential charge to extend from the ground to the leader tip. This column of charge, called a return stroke, travels with a velocity from one-tenth to one-third the speed of light up the ionized path that the leader created, reaching the cloud base in about 70 usec. The return stroke current typically reaches about 10 to 200 Kamps in a few microseconds and falls to half its peak value in about 20 to 60 usec. Currents on the order of hundreds of amperes may continue to flow for several milliseconds. If additional charge is available in the cloud after the return stroke,

the flash may contain additional strokes. These strokes usually begin with a dart leader propagating from the cloud to the earth along the already ionized path at a speed of about 2×10^6 m/sec, which is a magnitude faster than the stepped leader. The dart leader is then followed by another return stroke. If the ionized path is weakened after the return stroke by wind or a time lapse of more than 100 msec, then a dart-stepped leader may occur which alternates between the stepped and dart leader as it moves toward the earth.

Cloud discharges are the most frequently occuring form of lightning. They generally neutralize about the same amount of charge as a ground discharge, but are characterized by relatively smooth field changes as opposed to the ground return stroke. Also, the paths of cloud discharges are found to be more nearly horizontal than vertical. Although these differences may alter their statistics, the model of ARN will not distinguish between them for simplicity.

Propagation

Another important variable in the study of atmospherics is the effect of propagating medium between the flashes and the receiver. The characteristics of the medium are a function of the frequency of the emitting source, the propagation distance, and the reflective properties of the earth and ionosphere (Ref 12). The two common modes of propagation of low frequency radiation are the groundwave and waveguide modes. The groundwave has little effect on the receiver measurements because the antennas used to collect ARN data are placed well above the ground to avoid groundwave effects. The waveguide mode

results because of the complex conducting properties of the ionosphere and the earth. The waveguide mode of propagation allows radiation from distant storms to reach the receiver. The properties of atmospheric waveguide propagation have been summarized by Uman (Ref 16), Harth (Ref 5), and many others.

Power Spectrum

The leader and return stroke affect a different portion of the low frequency spectrum. The peak amplitude for the frequency spectrum of the return stroke generally occurs between 5 and 10 KHz. The peak amplitude of the frequency spectrum for the leader stroke is typically between 3 and 30 KHz. From about 10 KHz to 100 MHz, the peak electric field intensity of vertical polarized radiation from lightning varies approximately inversely with frequency (Ref 16).

In summary, the characteristics of ARN are sensitive to the frequency of operation and the location of the receiver. Since the sun affects the ionosphere, the characteristics of ARN are also affected by seasonal changes and the time of day. To represent ARN with a model, the model must have sufficient parameters to account for each of these factors. In the next chapter, a model will be presented which is based on the physical processes discussed in this chapter.

III. Point Process Model

An accurate noise model with a complete statistical description is very useful in receiver design and evaluation as well as in other aspects of electronic communication. Besides providing a complete description, the model must also be simple enough so that it can be traced through a mathematical representation of a receiver. Such a model would be a useful tool in the design and evaluation of receivers that must operate in that channel. In addition, the model must be validated to insure that the statistics of the model are in agreement with the statistics of the actual measured noise process. In this section, a model is proposed for which the complete statistical description is derived and a minimum probability of error receiver designed. The accuracy of the model will be investigated in the next chapter.

Development of the Proposed Model

Atmospheric noise consists of a highly impulsive component due to nearby return strokes during storm activity and a background noise that strongly resembles white Gaussian noise (Ref 15). The Gaussian noise is due to the large number of storms located far from the receiver plus the thermal and front end noise of the receiver. In the low frequency channel, the thermal and front end noise is usually negligible but it is important to note that the model can represent either type of noise. The highly impulsive noise component is assumed to be made up of lightning flashes as explained in Chapter II. Since

the lightning discharges are discrete events of a short time duration, it is reasonable to use a discrete time process to model them. Also, although multiple strokes during a flash may be correlated, the model will be designed under the assumption of uncorrelated strokes. This is done to preserve simplicity in the model and also because the correlation will have little effect on the first order distribution of the noise. The assumption of uncorrelated strokes indicates that a Poisson process may be a good model of the noise.

Another important characteristics of lightning that will affect the model is that the amplitude of the field at the receiver is different for each stroke. This can be modeled by defining a random mark for each Poisson arrival time. The random amplitude will be modeled as a zero mean Gaussian random variable.

The background Gaussian noise can be modeled by a similar process. This is so because when the rate of the Poisson process is high relative to the bandwidth of the receiver, the process observed at the output of the receiver will be indistinguishable from a Gaussian process (Ref 13).

Therefore, the proposed model of ARN consists of two separate marked Poisson processes. One process has a high rate and a low variance on the Gaussian marks to model the white Gaussian background noise. The other process has a low rate and a relatively high variance on the Gaussian marks to model the nearby highly impulsive ARN. The actual variance and rates of the two processes are parameters to be calculated for each specific situation to be modeled. The details of the parameters choise will be discussed in the validation study.

The resulting noise process is given below.

$$\underset{\sim}{n}(t) = \sum_{i=-\infty}^{\infty} \underset{\sim}{a}_i \delta(t-\underset{\sim}{\tau}_i) + \sum_{k=-\infty}^{\infty} \underset{\sim}{b}_k \delta(t-\underset{\sim}{\mu}_k) \qquad (1)$$

where

$n(t)$ is the ARN model

$\underset{\sim}{a}_i$ are the independent idnetically distributed Gaussian marks on the background process,

$\underset{\sim}{\tau}_i$ are the Poisson event times for the background process,

$\underset{\sim}{b}_k$ are the independent identically distributed Gaussian marks on the impulsive process,

$\underset{\sim}{\mu}_k$ are the Poisson event times for the impulsive process,

and

$\delta(\cdot)$ is the Dirac delta function.

In the next section section, this process will be used to derive the minimum probability of error processor for the channel.

Optimal Receiver Structure

The Bayes optimal processor for a given set of measurements is the processor that minimizes the expected cost associated with making a decision given the measurements. In this report, the optimal receiver will be a Bayes optimal binary hypothesis receiver with a symmetric cost function that is zero for a correct decision and some positive constant for an error. This minimum probability of error receiver is developed

in many texts (Ref 17). Given a set of measurements in the form of a random vector, Eq. (2) expresses the decision rule that will minimize the probability of error.

$$\frac{f_{\underset{\sim}{R}}(\underset{\sim}{R}|H_1)}{f_{\underset{\sim}{R}}(\underset{\sim}{R}|H_0)} \underset{H_0}{\overset{H_1}{\gtrless}} \frac{P_0}{P_1} \tag{2}$$

where

P_0 is the probability of hypothesis H_0

P_1 is the probability of hypothesis H_1

$\underset{\sim}{R}$ is the random measured vector,

and

$f_{\underset{\sim}{R}}(\underset{\sim}{R}|H_i)$ is the conditional joint density of the measurement vector given that signal S_i is sent for i=(0,1).

This expression is called the likelihood ratio test. The joint densities of the random measurement vector indicate the necessity for higher order statistics of the channel process to design the optimal receiver. For white Gaussian noise, the statistics are known from the first order density. This is not true for most other processes. Specifically, in the case of atmospheric radio noise, the joint density of a set of measurements is unsolved for the empirical models and complex for the proposed poisson process model.

In the following development, a minimum probability of error receiver for the low frequency channel is derived. The ARN model will be used to represent the noise in the channel.

The two signal hypotheses that the receiver must decide between are:

$$H_0: \underset{\sim}{r}(t) = S_0(t) + \underset{\sim}{n}(t) \tag{3}$$

$$H_1: \underset{\sim}{r}(t) = S_1(t) + \underset{\sim}{n}(t) \tag{4}$$

where

$\underset{\sim}{n}(t)$ is the ARN model

$\underset{\sim}{r}(t)$ is the measurement waveform

and

$S_0(t)$ and $S_1(t)$ are marked Poisson processes with known rate $\lambda_{s_j}(t)$ and known mark density $f_{\underset{\sim}{s}_j}(M)$.

In the following discussion, an optimal binery receiver using the decision rule in Eq. (2) will be derived.

The joint density of the marks, event times and the number of events is necessary for both hypotheses to implement the optimal decision rule. The joint density can be found by combining the individual Poisson processes into a single Poisson process. This is so because no two events can occur simultaneously in a Poisson process (Ref 13). The resulting density of a mark for the single Poisson process will be a mixture density. For hypothesis H_0, the mixture density can be written as,

$$f_{\underset{\sim}{M}_i}(M_i|t_i,H_0) = P[M_i \text{ came from the background process}|t_i]f_a(M_i)$$
$$= P[M_i \text{ came from the impulsive process}|t_i]f_{\underset{\sim}{b}}(M_i)$$
$$= P[M_i \text{ came from the signal process}|t_i]f_{\underset{\sim}{s}_0}(M_i)$$

It is implied by the subscript on the mark that the mark is associated with a Poisson event time. The probability that the mark came from a particular process is then determined by the relative rates of the processes at the event time associated with the mark.

$$f_{\underset{\sim}{M}_i}(M_i|t_i,H_j) = \frac{\lambda_a(t_i)f_a(M_i)+\lambda_b(t_i)f_{\underset{\sim}{b}}(M_i)+\lambda_{s_j}(t_i)f_{\underset{\sim}{s}_j}(t_i)}{\lambda_a(t_i)+\lambda_b(t_i)+\lambda_{s_j}(t_i)} \qquad (5)$$

The marks are independent of each other so the joint density on the marks over an interval of T given that N evetns occur is the product of the individual makr densities. The event time statistics for a Poisson process is given by Synder (Ref 13).

$$f_{\underset{\sim}{t},\underset{\sim}{N},\underset{\sim}{M}}(\underline{t},N,\underline{M}|H_j) = f_{\underset{\sim}{t},\underset{\sim}{N}}(t,N|H_j)f_{\underset{\sim}{M}}(\underline{M}|\underline{t},\underline{N},H_j)$$

$$= \prod_{i=1}^{N}[\lambda_a(t_i)+\lambda_b(t_i)+\lambda_{s_j}(t_i)]. \qquad (6)$$

$$\exp\left[-\int_0^T \lambda_a(t)+\lambda_b(t)+\lambda_{s_j}(t)dt\right]$$

$$\cdot \prod_{i=1}^{N} \frac{\lambda_a(t_i)f_{\underset{\sim}{a}}(M_i)+\lambda_b(t_i)f_{\underset{\sim}{b}}(M_i)+\lambda_{s_j}(t_i)f_{\underset{\sim}{s_j}}(M_i)}{\lambda_a(t_i)+\lambda_b(t_i)+\lambda_{s_j}(t_i)} \tag{7}$$

By writing the product of a ratio by the ratio of products the denominator will cancel and yield

$$f_{\underset{\sim}{t},\underset{\sim}{N},\underset{\sim}{M}}(\underset{\sim}{t},N,\underset{\sim}{M}\ H_j) = \prod_{i=1}^{N}[\lambda_a(t_i)f_{\underset{\sim}{a}}(M_i)+\lambda_b(t_i)f_{\underset{\sim}{b}}(M_i)+\lambda_{s_j}(t_i)f_{\underset{\sim}{s_j}}(M_i)]$$

$$\cdot \exp\left[\int_0^T \lambda_a(t)+\lambda_b(t)+\lambda_{s_j}(t)dt\right] \tag{8}$$

The resulting likelihood ratio after taking the natural log of both sides to change the products to sums, is given by,

$$\sum_{i=1}^{N}\{\ln[\lambda_a(t_i)f_{\underset{\sim}{a}}(M_i)+\lambda_b(t_i)f_{\underset{\sim}{b}}(M_i)+\lambda_{s_1}(t_i)f_{\underset{\sim}{s_j}}(M_i)]$$

$$-\ln[\lambda_a(t_i)f_{\underset{\sim}{a}}(M_i)+\lambda_b(t_i)f_{\underset{\sim}{b}}(M_i)+\lambda_{s_0}(t_i)f_{\underset{\sim}{s_0}}(M_i)]\}$$

$$\begin{matrix} H_1 \\ > \\ < \\ H_0 \end{matrix} \ln\left(\frac{P_0}{P_1}\right) + \int_0^T [\lambda_{s_1}(t) - \lambda_{s_0}(t)]dt \qquad (9)$$

The processor therefore turns out to be nonlinear. This means that there is no linear correlation receiver that can implement the processor.

To determine if this processor is optimal for the low frequency channel, the ARN model must be checked for its representation of the noise. In the next chapter, a validation study will confirm the accuracy of the ARN model.

IV. Verification of ARN Model

A noise model must be proven accurate in order to be used with confidence. In this chapter, the first order statistics of the proposed model will be compared to those of measured data. The measured data is in the form of the amplitude probability distribution (APD) of the envelope of ARN detected by a finite bandwidth receiver. APD curves measured by this type of receiver are presented in two articles that will be addressed in this chapter. They are (1) K. Furutsu and T. Ishida (Ref 3), and (2) CCIR report 322 (Ref 22). If, through a choice of parameters for the model, the mean square error (MSE) is small between the theoretical APD curve given by Eq. (39) and a measured APD curve, then the model will be assumed to be a good representation of ARN. In other words, if the first order statistics of the model are close to those of ARN, then the higher order statistics will be assumed to be close also. This is a reasonable assumption because the process model is based on the physics of the noise process as was discussed earlier.

This chapter consists of four sections. First, (1) the noise model will be used as an input to a mathematical representation of a finite bandwidth envelope detector. The resulting APD of the envelope at the output of the receiver will be used for validation. Next, (2) the MSE criterion for measuring the error between the measured and theoretical APD curves will be discussed. Then (3)

the Furutsu and Ishida data will be compared to the theoretical APD curves. This section will include a summary of the Furutsu and Ishida article plus a discussion of the parameter values and their relation to the parameters discussed in the article. Finally, (4) the data will be compared to the data contained in CCIR report 322. This section will also include a brief discussion of parameter choice. A summary of CCIR report 322 is included in Appendix A (Ref 6).

In the next section, the APD of the output of a quadrature receiver is derived for the ARN model.

Verification of the Point Process Model

To verify the point process model, it will be used as an input to a representation of the receiver used in the CCIR report 322 and the K. Furutsu and T. Ishida article. Both receivers are envelope detectors with a finite bandwidth. A representation of this type of receiver is shown in Figure 1. The representation will be referred to as the receiver in the following developments. The receiver consists of quadrature multipliers followed by integrators to represent the bandpass filter (Ref 13). The envelope of the quadrature components, $\underset{\sim}{n}_1$ and $\underset{\sim}{n}_2$, is then detected by the square root of the sum of squares of the quadrature components. In this section, the proposed process is used as an input to the quadrature receiver described. The resulting statistics of the envelope at the output will then

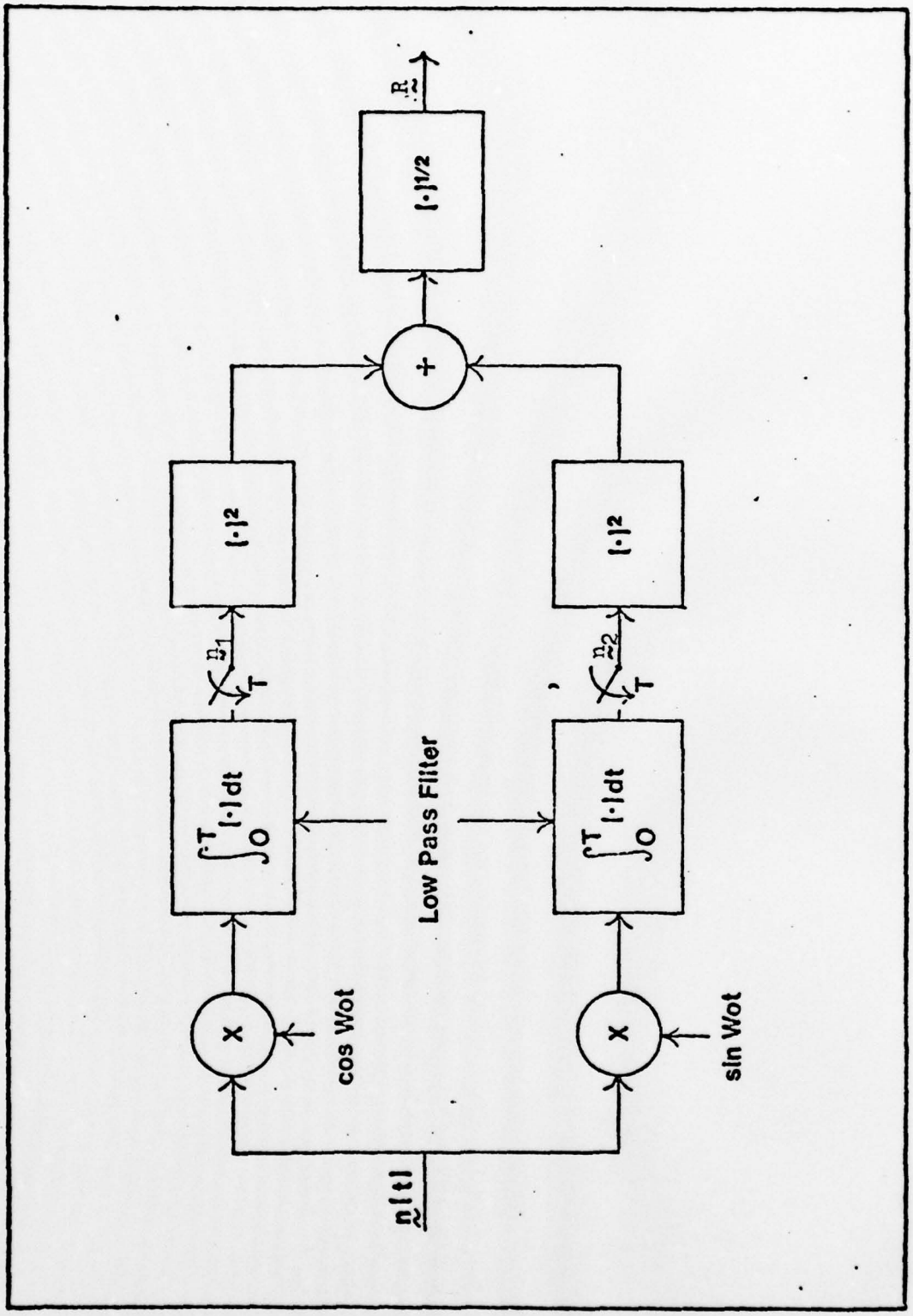

Fig. 1. Quadrature Receiver

be compared to those of the CCIR report 322 and the Furutsu article after choosing the appropriate parameters. If, through a choice of parameters, the first order statistics of the model are close to those of the measured data, the higher order statistics will be assumed to be close also. The measure of closeness or fit of the data will be discussed later in this section.

The input process to the receiver is defined in Eq. (1). The output of the integrators of Figure 2 is then,

$$\underset{\sim}{n}_1 = \int_0^T \underset{\sim}{n}(t) \cos \omega_0 t \, dt \tag{10}$$

$$\underset{\sim}{n}_2 = \int_0^T \underset{\sim}{n}(t) \sin \omega_0 t \, dt \tag{11}$$

Substituting for $\underset{\sim}{n}(t)$ in Eq. (16),

$$\underset{\sim}{n}_1 = \int_0^T \sum_{i=\infty}^{\infty} \underset{\sim}{a}_i \delta(t-\underset{\sim}{\tau}_i) \cos \omega_0 t \, dt$$

$$+ \int_0^T \sum_{k=-\infty}^{\infty} \underset{\sim}{b}_k \delta(t-\underset{\sim}{\mu}_k) \cos \omega_0 t \, dt \tag{12}$$

By intercahnging summation and integration and using the sifting property of the delta function,

$$\underset{\sim}{n}_1 = \sum_{i=0}^{\underset{\sim}{N}_a} \underset{\sim}{a}_i \cos \omega_0 \underset{\sim}{\tau}_i + \sum_{k=0}^{\underset{\sim}{N}_b} \underset{\sim}{b}_k \cos \omega_0 \underset{\sim}{\mu}_k \tag{13}$$

Where

$\underset{\sim}{N}_a$ and $\underset{\sim}{N}_b$ are the number of events which occur in time T for the $\underset{\sim}{a}$ and $\underset{\sim}{b}$ processes respectively. Also,

$$\underset{\sim}{n}_2 = \sum_{i=0}^{\underset{\sim}{N}_a} \underset{\sim}{a}_i \sin \omega_0 \underset{\sim}{\tau}_i + \sum_{k=0}^{\underset{\sim}{N}_b} \underset{\sim}{b}_k \sin \omega_0 \underset{\sim}{\mu}_k \tag{14}$$

The problem is to find the envelope density of the $\underset{\sim}{n}_1$ and $\underset{\sim}{n}_2$ quadrature components. The $\underset{\sim}{\mu}_k$ and $\underset{\sim}{\tau}_i$ are ordered event times distributed uniformly on (0,T). Usually, $T \gg 1/\omega_0$. If this is not true then it must be assumed that $\underset{\sim}{\mu}_k$ and $\underset{\sim}{\tau}_i$ are uniformly distributed on $(0,2n\pi)$ for integer $n>0$. Also, from the definition of the marks, each corresponding pair of terms in $\underset{\sim}{n}_1$ and $\underset{\sim}{n}_2$ are independent of all other pairs of terms. Defining $\underset{\sim}{X}$ and $\underset{\sim}{Y}$ to represent a typical pair of terms in the summations for $\underset{\sim}{n}_1$ and $\underset{\sim}{n}_2$,

$$\underset{\sim}{X} = \underset{\sim}{a} \cos \omega_0 \underset{\sim}{\tau} \tag{15}$$

and

$$\underset{\sim}{Y} = \underset{\sim}{a} \sin \omega_0 \underset{\sim}{\tau}. \tag{16}$$

The joint density of $\underset{\sim}{X}$ and $\underset{\sim}{Y}$ can be written as,

$$f_{\underset{\sim}{X},\underset{\sim}{Y}}(X,Y|a) = \frac{1}{2\pi R}(R-|a|) \quad \text{(Ref 9:174)} \tag{17}$$

where

$$R = \sqrt{X^2 + Y^2}$$

and

$\delta(R-|a|)$ represents the probability line mass $f_{\underset{\sim}{X},\underset{\sim}{Y}}(X,Y)$ located on the circle $X^2+Y^2=a^2$.

The characteristics function of thejoint density on $\underset{\sim}{X}$ and $\underset{\sim}{Y}$ can now be written as,

$$\psi_{\underset{\sim}{X},\underset{\sim}{Y}}(\rho,\phi|\underline{a}) = \frac{1}{2\pi}\int_0^{2\pi}\int_0^{\infty} f_{\underset{\sim}{X},\underset{\sim}{Y}}(R,\theta|\underset{\sim}{a})$$

$$\cdot \exp[jR\rho\cos(\theta-\phi)]RdRd\theta \tag{18}$$

where

$$\theta = \tan^{-1}\left(\frac{X}{Y}\right)$$

This is the joint characteristic function for the random variables $\underset{\sim}{X}$ and $\underset{\sim}{Y}$, even though this integral is evaluated in polar coordinates. By the sifting property of the delta function,

$$\psi_{\underset{\sim}{X},\underset{\sim}{Y}}(\rho,\phi|a) = \frac{1}{2\pi}\int_0^{2\pi} \exp[ja\rho \cos(\theta-\phi)]\, d\theta$$

$$= J_0(a\rho) \tag{19}$$

where $J_0(\cdot)$ is the zero order Bessel function of the first kind. Each corresponding pair of terms in $\underset{\sim}{n}_1$ and $\underset{\sim}{n}_2$ will be independent of all other pairs of terms in the summations. This allows the joint density on $\underset{\sim}{n}_1$ and $\underset{\sim}{n}_2$ to be written as the N-fold convolution of the joint density on each pair. In the characteristic function domain, this convolution can be written as a product. Writing the joint characteristic function of $\underset{\sim}{n}_1$ and $\underset{\sim}{n}_2$ as the product of the joint characteristic function of each succeeeding pair of random variables in the summation yields,

$$\psi_{\underset{\sim}{n}_1,\underset{\sim}{n}_2}(\rho,\phi|a_i,b_k,N_a,N_b) = \prod_{i=1}^{N_a} J_0(a_i\rho) \prod_{k=1}^{N_b} J_0(b_k\rho) \tag{20}$$

To remove the conditioning on $\underset{\sim}{a}_i$, $\underset{\sim}{b}_k$, $\underset{\sim}{N}_a$, and $\underset{\sim}{N}_b$, the characteristics function can be averaged over the statistics of $\underset{\sim}{a}_i$, $\underset{\sim}{b}_k$, $\underset{\sim}{N}$, and $\underset{\sim}{N}_b$ respectively. Since each term in the first and second products is independent of all other terms, the averages can be done for each term individually.

$$\int_{-\infty}^{\infty} J_0(a\rho)\, f_{\underset{\sim}{a}}(a)\, da$$

$$= \int_{-\infty}^{\infty} J_0(a\rho) \frac{1}{\sqrt{2\pi}\sigma_a} \exp\left[\frac{-a^2}{2\sigma_a^2}\right] da$$

$$= \exp\left[\frac{-\rho^2\sigma_a^2}{4}\right] I_0\left[\frac{\rho^2\sigma_a^2}{4}\right] \qquad \text{(Ref 7:313]} \qquad (21)$$

where I_0 is the zero order modified Bessel function. Performing the same average over the statistics on eack $\underset{\sim}{b}_k$ term leads to the following result.

$$\Psi_{\underset{\sim}{n}_1,\underset{\sim}{n}_2}(\rho,\phi|N_a,N_b) = \left[\exp\left(\frac{-\rho^2\sigma_a^2}{4}\right) I_0\left(\frac{\rho^2\sigma_a^2}{4}\right)\right]^{N_a}$$

$$\cdot \left[\exp\left(\frac{-\rho^2\sigma_b^2}{4}\right) I_0\left(\frac{\rho^2\sigma_b^2}{4}\right)\right]^{N_b} \qquad (22)$$

The average over the statistics of $\underset{\sim}{N}_a$ and $\underset{\sim}{N}_b$ can be done next.

$$\psi_{\underset{\sim}{n}_1,\underset{\sim}{n}_2}(\rho,\phi) = \sum_{i=1}^{\infty}\left[\sum_{j=1}^{\infty}\psi_{\underset{\sim}{n}_1,\underset{\sim}{n}_2}(\rho,\phi|\underset{\sim}{N}_a=j,\underset{\sim}{N}_b=i)p(\underset{\sim}{N}_a=j)\right]p(\underset{\sim}{N}_b=i) \tag{23}$$

where

$$P(\underset{\sim}{N}_a=j) = \frac{(\lambda_a T)^j \exp(-\lambda_a T)}{j!} \quad , \tag{24}$$

$$P(\underset{\sim}{N}_b=i) = \frac{(\lambda_b T)^i \exp(-\lambda_b T)}{i!} \tag{25}$$

and

T is the integration time of the receiver.

Performing the required average uields,

$$\psi_{\underset{\sim}{n}_1,\underset{\sim}{n}_2}(\rho,\phi) = \sum_{i=0}^{\infty}\left[\sum_{j=0}^{\infty}\frac{[\lambda_a T I_0(\frac{\rho^2\sigma_a^2}{4})\exp(\frac{-\rho^2\sigma_a^2}{4})]^j \exp(-\lambda_a T)}{j!}\right.$$

$$\left.\cdot \exp[I_0(\frac{\rho^2\sigma_b^2}{4})\exp(\frac{-\rho^2\sigma_b^2}{4})]^i\right]\frac{(\lambda_b T)^i \exp(-\lambda_b T)}{i!}$$

$$= \exp[\lambda_a T\ I_0(\frac{\rho^2\sigma_a^2}{4})\exp(\frac{-\rho^2\sigma_a^2}{4})]\exp(-\lambda_a T)$$

$$\cdot \exp[\lambda_b T\ I_0(\frac{\rho^2\sigma_b^2}{4})\exp(\frac{-\rho^2\sigma_b^2}{4})]\exp(-\lambda_b T)$$

$$= \exp\left\{-T(\lambda_a+\lambda_b)+T[\lambda_a I_0(\frac{\rho^2\sigma_a^2}{4})\exp(\frac{-\rho^2\sigma_a^2}{4})\right.$$

$$\left. + \lambda_b I_0(\frac{\rho^2\sigma_b^2}{4})\exp(\frac{-\rho^2\sigma_b^2}{4})]\right\} \qquad (26)$$

The unconditional joint density on $\underset{\sim}{n}_1$ and $\underset{\sim}{n}_2$ can be found from the unconditional characteristic function through the transform defined below.

$$f_{\underset{\sim}{n}_1,\underset{\sim}{n}_2}(R,\theta) = \frac{1}{(2\pi)^2}\int_0^\infty\int_0^{2\pi}\exp[-jR\rho\cos(\phi-\theta)] \qquad (27)$$

$$\cdot \Psi_{\underset{\sim}{n}_1,\underset{\sim}{n}_2}(\rho,\phi)\rho d\rho d\phi$$

where

R is now defined as $\sqrt{n_1^2+n_2^2}$

and

$$\theta = \tan^{-1}\left(\frac{n_2}{n_1}\right)$$

$$f_{\underset{\sim}{n}_1,\underset{\sim}{n}_2}(R,\theta) = \frac{1}{2\pi}\int_0^{\infty} J_0(\rho R)\psi_{\underset{\sim}{n}_1,\underset{\sim}{n}_2}(\rho)\rho d\rho \qquad (28)$$

because $\psi_{\underset{\sim}{n}_1\underset{\sim}{n}_2}(\rho,\phi)$ is independent of ϕ.

Since the envelope statistics are required, it is necessary to convert the joint density on $\underset{\sim}{n}_1$ and $\underset{\sim}{n}_2$ to a joint density on $\underset{\sim}{R}$ and $\underset{\sim}{\theta}$ where,

$$R = \sqrt{\underset{\sim}{n}_1^2+\underset{\sim}{n}_2^2} \qquad (29)$$

and

$$\underset{\sim}{\theta} = \tan^{-1}\left(\frac{\underset{\sim}{n}_2}{\underset{\sim}{n}_1}\right)$$

$$f_{\underset{\sim}{R},\underset{\sim}{\theta}}(R,\theta) = Rf_{\underset{\sim}{n}_1,\underset{\sim}{n}_2}(R\cos\theta,\ R\sin\theta)$$

$$= \frac{R}{2\pi}\int_0^{\infty} J_0(\rho R)\psi_{\underset{\sim}{n}_1,\underset{\sim}{n}_2}(\rho)\rho d\rho \qquad (30)$$

The cumulative distribution on the envelope is then given by,

$$F_{\underset{\sim}{R}}(R_0) = \int_0^{R_0}\int_0^{2\pi} f_{\underset{\sim}{R},\underset{\sim}{\theta}}(R,\theta)dRd\theta$$

$$= \int_0^{\infty}\left[\int_0^{R_0} RJ_0(\rho R)dR\right]\rho\psi_{\underset{\sim}{n}_1,\underset{\sim}{n}_2}(\rho)\ d\rho$$

$$= \int_0^{\infty}\frac{R_0 J_1(\rho R_0)}{\rho}\rho\Psi_{\underset{\sim}{n}_1,\underset{\sim}{n}_2}(\rho)\ \ d\rho \qquad \text{(Ref 7)}$$

$$= \int_0^{\infty} R_0 J_1(\rho R_0)\,\psi_{\underset{\sim}{n}_1\underset{\sim}{n}_2}(\rho)\ d\rho \qquad (31)$$

The amplitude probability distribution (APD) is then defined by $1-F_{\underset{\sim}{R}}(R_0)$ which is,

$$1 - F_{\underset{\sim}{R}}(R_0) = 1-\int_0^{\infty} R_0 J_1(\rho R_0)\exp[-T(\lambda_a+\lambda_b)+T(\lambda_a I_a(\frac{\rho^2\sigma_a^2}{4})$$

$$\cdot \exp(\frac{-\rho^2\sigma_a^2}{4}) + \lambda_b I_0(\frac{\rho^2\sigma_b^2}{4})\exp(\frac{-\rho^2\sigma_b^2}{4})]d\rho \qquad (27)$$

This expression can be numerically integrated for values of R_0 to plot the APD curve for a set of given parameter values. The method of integration is discussed in Appendix B.

This APD will be compared to measured APD curves for different parameter values. The comparison will be based on a Mean Square Error (MSE) distance between the curves. This distance is discussed in the next section.

MSE Criterion

A quantitative measurement of error between APD curves must be established to compare the theoretical and measured APD curves. The APD curve is a plot of threshold value versus the probability that the envelope of the noise exceeds the threshold value. This is plotted on Rayleigh paper which forces the Rayleigh distribution to plot as a straight line. The criterion to be used to measure the MSE between curves is defined below.

$$MSE = \frac{\sum_{i=1}^{N} (d_i)^2}{N} \tag{28}$$

Where

MSE is the sample mean square error between the APD curves,

d_i is the linear distance between the curves on Rayleigh paper for a given threshold value as given by Eq. (29).

$$d_i = LOG_{10}\left[\frac{\ln(P_{Mi})}{\ln(P_{Ti})}\right] \tag{29}$$

P_{MI} is the probability that a measured value exceeds the threshold Δ_i.

P_{TI} is the probabiliy that a theoretical value exceeds the threshold Δ_i.

and

N is the number of samples to be taken from the curves.

In the following section, the Furutsu and Ishida article is discussed and two measured APD curves are compared to theoretical APD curves of the ARN model.

Summary of K. Furutsu and T. Ishida Article

K. Furutsu and T. Ishida have developed a model of atmospheric noise which consists of a Poison-Poison process (Ref 3). A

Poison-Poison process is a Poisson process that is amplitude modulated by a function that occurs according to the event times a Poisson process of another rate. They based this model on the natural processes involved in lightning, the major source of atmospheric noise. The predischarge (stepped leader) consists of many random impulses of the order of duration of 1 usec, each of which occur successively in the time interval of 25 to 100 usec. This indicates that the predischarge, which would occur in time according to a Poisson distribution, forms a wave packet of Poisson noise. In the paper, these packets have an envelope of a growing exponential which reaches a finite value and then returns to zero.

The process is then validated by comparing the theoretical first order density to the measured first order density of the output of an envelope detector with a finite bandwidth. The receiver detects the amplitude waveform with a bandpass filter and then measures the amplitude distribution of the envelope.

Two cases are used for the validation study. One case assumes that the noise is created by a strong local source at a short distance and that other sources are continuously distributed far distant so that the noise strength is much lower for the distant sources starting at some distance from the receiver and extending to infinity. The amplitude of the noise varies inversely with the distance from the receiver. It is clear from their study that there is strong correlation between their model and the measured ARN.

Comparison to Furutsu and Ishida Data

To begin the comparison, the parameters of the theoretical model developed in Chapter III must be chosen. Since the model that Furutsu and Ishida developed is related to the Poisson process, the parameters that they specify for the measured APD curves are directly applicable to the model of Chapter III. The parameters of the two APD curves in Figs. 2 and 3 are given in Table I. The only parameter that had to be experimentally determined was the rate of the background process. It was found that a rate of about 1.5 to 1.8 times the bandwidth of the filter was sufficient to produce good agreement. In the Furutsu and Ishida curves the envelope threshold (plotted vertically for the two plots) was in terms of a ratio of the envelope threshold to the standard deviation of the background noise. Therefore, the background noise for the point process model is chosen to be 1. This allows both curves to be easily plotted on the same scale. The other parameters are defined in terms of two other ratios. The ratios are (1) the rate of the impulsive process divided by the bandwidth of the IF filter and (2) the standard deviation of the impulsive noise divided by the standard deviation of the background noise. The second ratio is expressed in terms of decibels where,

$$\text{value in Db} = 20 \log_{10} (\text{ratio})$$

In addition to these parameters, the integration time was chosen by assuming that the integrator is approximately an ideal bandpass filter and that the double sided bandwidth is 2/T. T is the integration time. Actually, the integrators have a sinc shaped respone in the

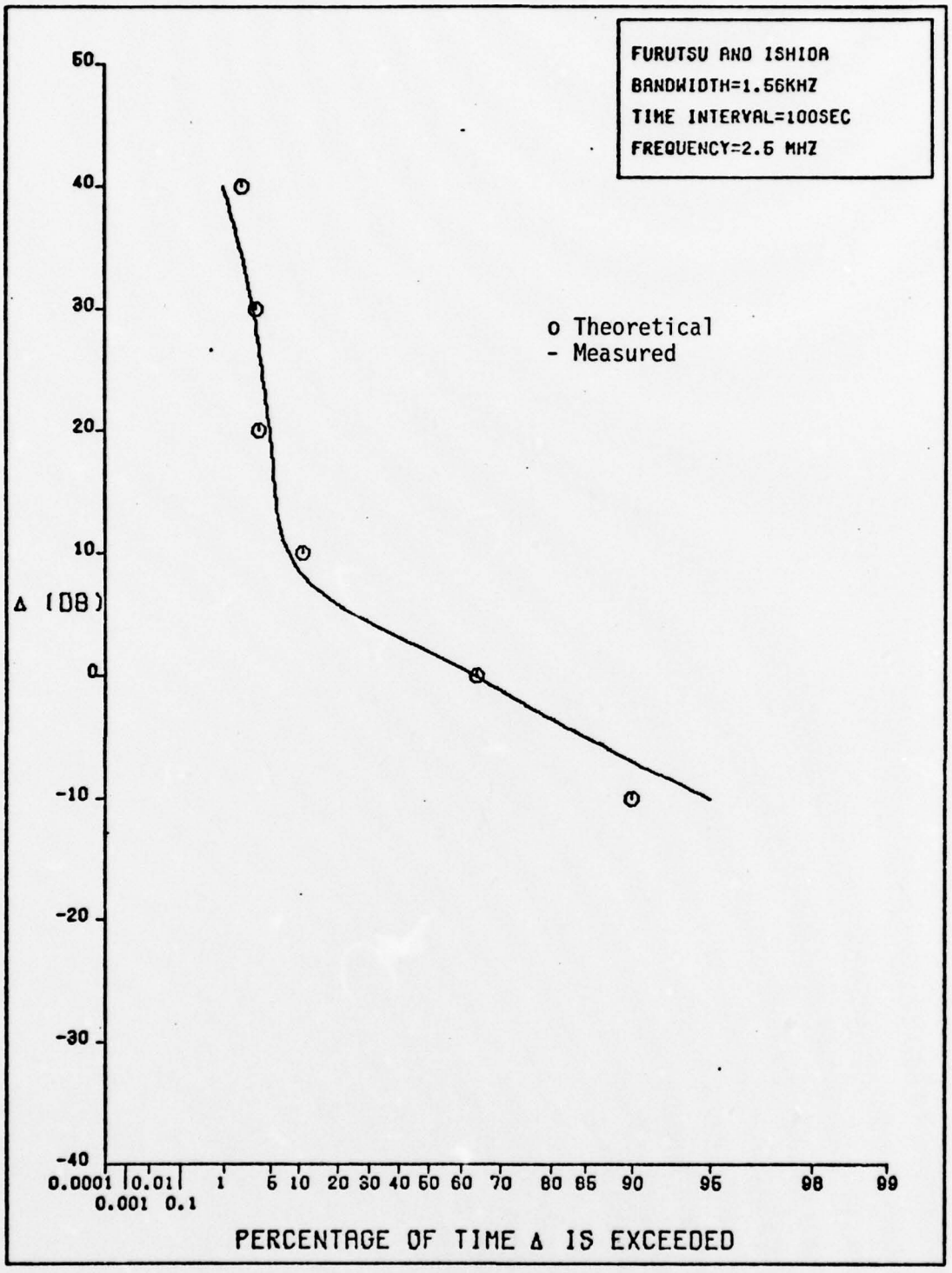

Fig. 2. Comparison of Measured and ARN Model APD Curves (MSE=.018)

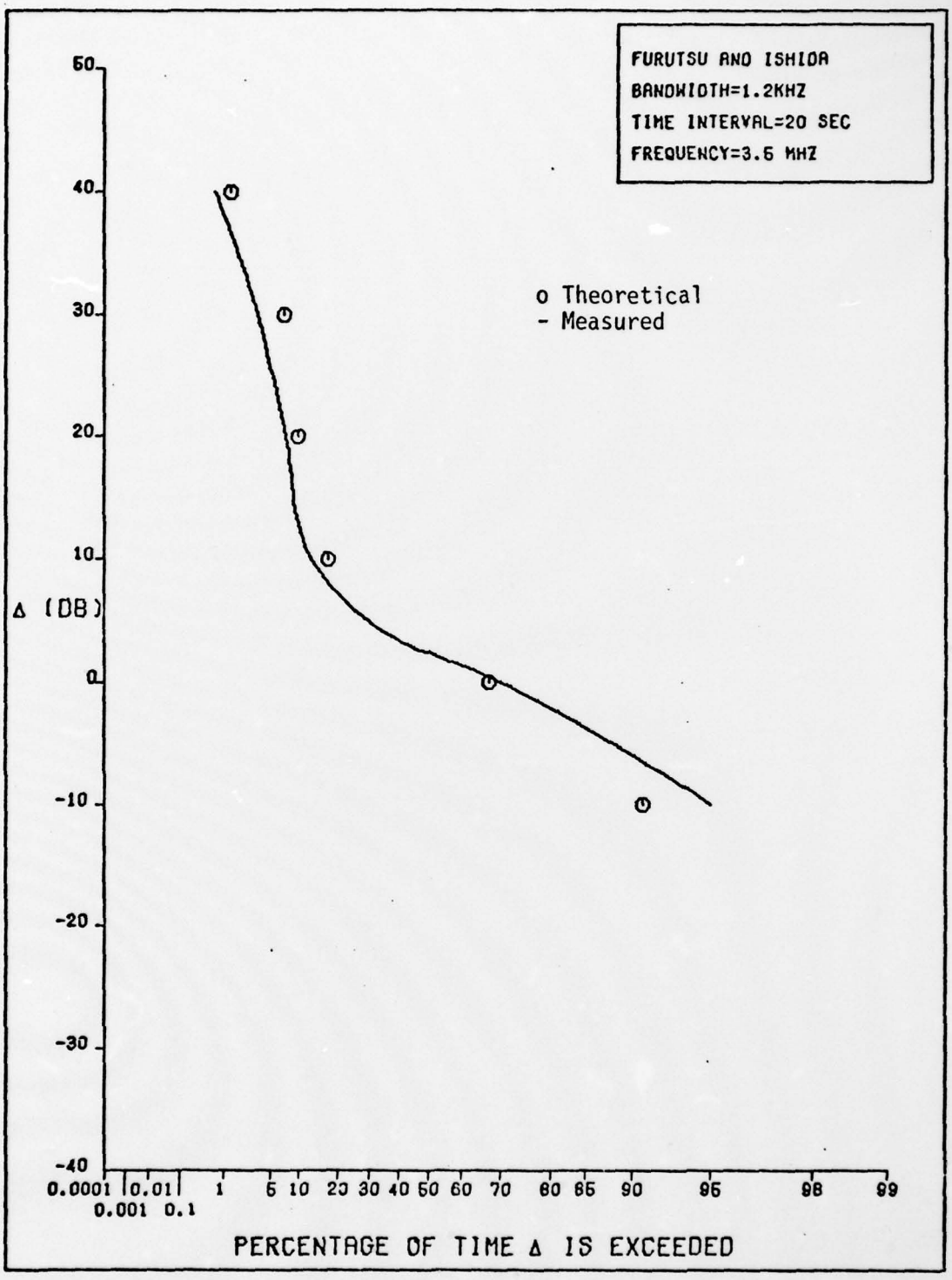

Fig. 3. Comparison of Measured and ARN Model APD Curves (MSE=.016)

frequency domain but close agreement was found using this approximation.

TABLE I

PARAMETERS FOR THE ARN MODEL

Figure	λ_a	λ_b	σ_a	σ_b	T
3	2500.0	30.4	1.0	158.5	.00132
4	2000.0	72.0	1.0	63.0	.00167
5	350.0	20.0	.11	2.0	.01

It is found that the theoretical curves from the point process developed in Chapter III are a very close fit to those of the measured data in the Furutsu and Ishida report. This is significant because the data was taken in the daytime with nearby storms. This indicates that the known correlation between strokes for nearby storms is adequately represented in the first order statistics derived from the model. Next, a similar comparison to the CCIR report 322 data will be made.

Comparison to CCIR Report 322 Data

In CCIR Report 322, measured ARN data from 16 receiving stations located around the world is collected and averaged. A summary of the report is given by Hettinger (Ref 6) in Appendix A. Several APD curves are given in the report and each is specified by only a V_d ratio which is a measure of the impulsiveness of the noise. The definition of this ratio is given in Eq. (A4). To relate the parameters of the point process model to this ratio would require

computations of ensemble averages. The averages were not computed due to the time constraints of this project (they require numerical integrations). Since the parameters of the model could not be directly related to the V_d ratio, each parameter was determined by the parameter's effect on the resulting theoretical APD curve. The rate of the background proces was set to 1.75 times the bandwidth, which was determined in the Furutsu and Ishida comparison. Also, an article by Spauling et al. (Ref 15) indicated that the lower portion of the curve is determined by the background noise and the upper portion is determine by the impulsive noise. Therfore, a change in the variance of the background process marks produced a fit to the lower portion of the curve. The upper portion of the curve was then matched by a variation of both the rate and variance of the impulsive process. Although this may seem arbitrary, for given ARN the rate of the impulsive process can be determined by observing the number of large fluctuations in the envelope of the noise in a given time. The variance can then be used to adjust the power of the model so that it matches the noise power.

The plot shown in Figure 4 shows that for the chosen parameter values the model acurately represents the first order statistics of ARN as given for V_d=8 in the CCIR report.

The point process model is therefore found to be versatile in its ability to represent the first order statistics of ARN. The parameters of the model can be chosen to represent a variety of situations, of which three are shown here.

It is interesting to note that if other types of noise that are not correlated with the ARN or each other are significant, the

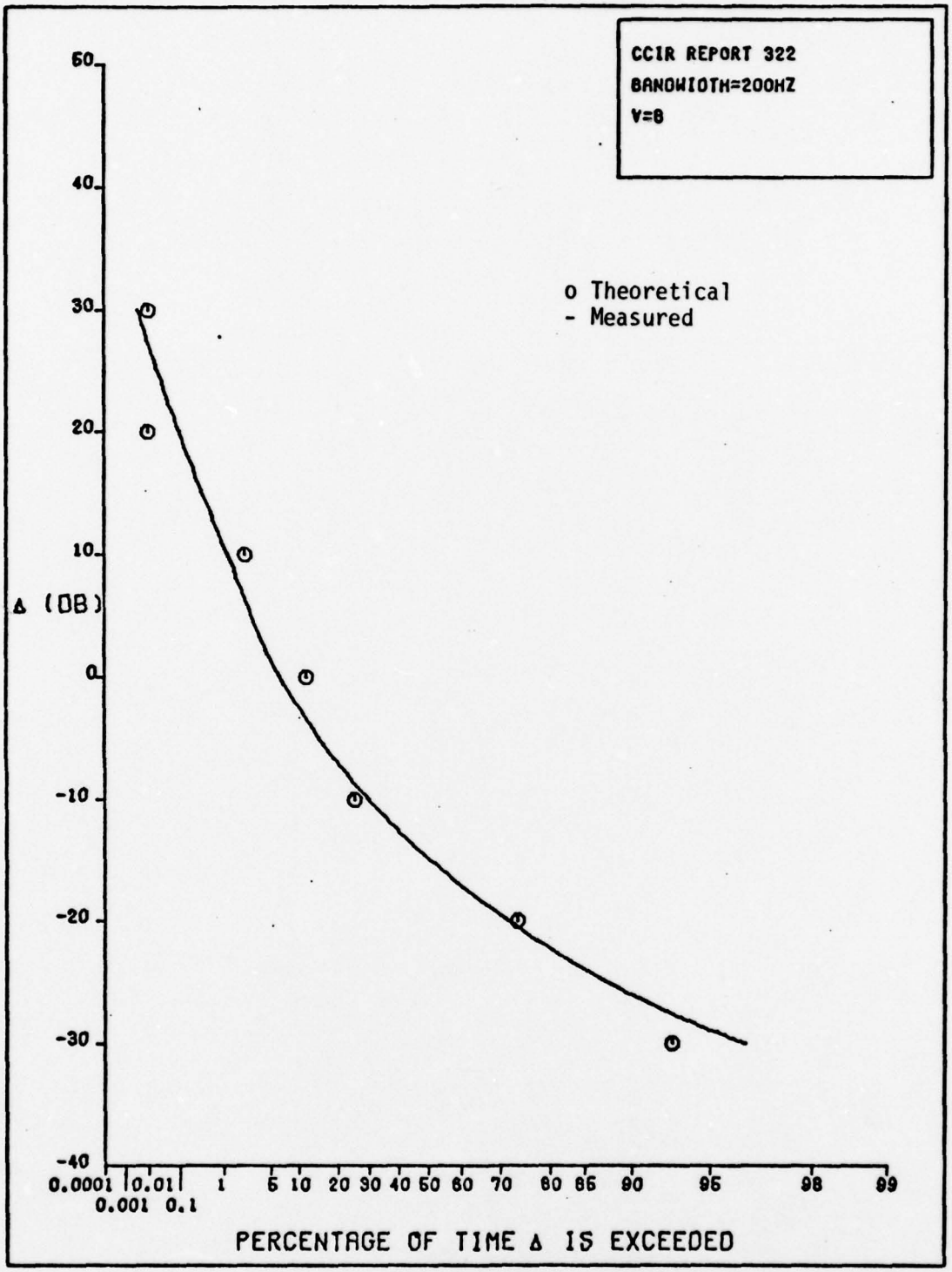

Fig. 4. Comparison of Measured and ARN Model APD Curves (MSE=.018)

model allows as many marked point processes as are necessary to be added wthout increasing the complexity of the analysis done in this report. This is another useful feature of the model. In the next chapter, some suggestions will be made for further studies along with some conclusions about the point process model.

V. Conclusions and Rcommendations

In conclusion, a sum of marked Poisson processes is a good representation of ARN. The ARN model developed in this report was the sum of two marked point processes, each with zero mean Gaussian marks. Even with this simplified structure, the model was found to be in good agreement with the measured first order distribution of ARN. The simplified structure constitutes a tractable model that can be traced through a quadrature receiver, and results in the design of a Bayes optimal binary receiver for the channel.

It is recommended that further studies of this model be directed to two areas. These are (1) a more thorough validation should be done with raw data. This validation should involve higher order statistics of the process and should determine the useful range of the model. (2) Performance evaluations should be done for both optimal receivers designed for the low frequency channel and the suboptimal receivers presently being used in the low frequency channel. These performance evaluations should be done using the marked Poisson process model as the input noise to the receivers. This will allow bounds on the performance of the receivers to be determined along with a comparison of receivers presently in use.

Bibliography

1. Crichlow, W. Q., et al. Amplitude Probability Distributions for Atmospheric Radio Noise. National Bureau of Standards Monograph 23, PB183992. Washington, D. C.: Department of Commerce, November 1960.

2. -----. "Determination of the Amplitude-Probability Distribution of Atmospheric Radio Noise from Statistical Moments," Journal of Research of National Bureau of Standards--D. Radio Propagation, 64D (1): 49-56 (1960).

3. Furutsu, K. and T. Ishida. "On the Theory of Amplitude Distribution of Impulsive Random Noise," Journal of Applied Physics, 32 (7): 1206-1221 (1963).

4. Gagliardi, Robert M. and Sherman Karp. Optical Communications. New York: John Wiley and Sons Inc., 1976.

5. Harth, W. "Physics of Lightning and SFERICS, Part II," International Conference of Electrical Processes in Atmospheres. Darmstadt, West Germany 1977.

6. Hettinger, Steven D. A Random Point Process Model for Atmospheric Radio Noise. MS Thesis. Wright-Patterson AFB, Ohio: Air Force Institute of Technology, March 1978.

7. Luke, Yudell L. Integrals of Bessel Functions. New York: McGraw Hill Book Company, 1962.

8. Macchi, Odile and Bernard C. Picinbono. "Estimation and Detection of Weak Optical Signals," IEEE Transactions on Information Theory, vol IT-18, no 5, September 1972.

9. Papoulis, Anthanasios. Probability, Random Variables, and Stochastic Processes. New York: McGraw-Hill Book Company, 1965.

10. -----. Systems and Transforms with Applications in Optics. New York: McGraw-Hill Book Company, 1968.

11. Reed, I.S. "On a Moment Theorem for Complex Gausian Processes," Ire Transactions on Information Theory, vol IT-8, no 3, April 1962.

12. Rustan, P.L. "Properties of Lightning Derived from Time Series Analysis of VHF Radiation Data," University Microfilms, Dissertation International, University of Florida, 1977.

13. Snyder, Donald L. Random Point Processes. New York: John Wiley and Sons Inc., 1975.

14. Spaulding, Arthur D. and David Middleton. "Optimum Reception in an Impulsive Interference Environment--Part I: Coherent Detection, IEEE Transactions on Communications, vol COM-25, no 9, September 1977.

15. Spaulding, A. D. "Conversion of the Amplitude-Probability Distribution of Atmospheric Radio Noise from One Bandwidth to Another," Journal of Research of National Bureau of Standards--D. Radio Propagation, 66D (6): 713-720 (1962).

16. Uman, Martin A. Lightning. New York: McGraw-Hill Book Company, 1969.

17. Van Trees, Harry L. Detection, Estimation and Modulation Theory, Part I. New York: John Wiley and Sons Inc., 1968.

18. -----. Detection, Estimation, and Modulation Theory, Part III. New York: John Wiley and Sons Inc., 1971.

19. Wilson, Kenneth E. Analysis of the Crichlow Graphical Model of Atmospheric Radio Noise at Very Low Frequencies. MS Thesis. Wright-Patterson AFB, Ohio: Air Force Institute of Technology, November 1974. AD-A008679.

20. Wozencraft, John M. and Irwin M. Jacobs. Principles of Communication Engineering. New York: John Wiley and Sons Inc., 1965.

21. -----. "Noise Investigation at VLF by the National Bureau of Standards," Proceedings of the IRE, 42: 778-783 (June 1957).

22. -----. World Distribution and Characteristics of Radio Noise. CCIR Report 322. Geneva: International Telecommunication Union, 1964.

Appendix A: Summary of CCIR Report 322 by Hettinger (Ref 6)

A large quantity of ARN data has been gathered by the National Bureau of Standards. This data includes worldwide time averaged noise power measurements, and amplitude probability distribution curves for the time varying noise envelope. This work is presented in condensed form in CCIR Report 322 (Ref 22). The block diagram of the receiver used in these measurements is presented in Figure A1.

The worldwide measurements of ARN power are derived from measurements made by sixteen receiving stations throughout the world. Figure A2 shows the location of these stations. The average noise power available at the antenna is relatively constant for observation intervals up to four hours. The measurements made during these four-hour periods are relatively constant from day-to-day for periods up to three months. Therefore, the noise power measurements in CCIR Report 322 are plotted for the four seasons of the year, and each seasonal section contains six plots of the four hour time blocks in a day (Ref 22). Figure A3 shows a typical average noise power plot from CCIR Report 322. The average noise figure, F_a, shown in Figure A3 is computed from Eq (A1).

$$F_a = 10 \text{ Log}_{10} \frac{\left[\frac{1}{T}\int_0^T E^2(t)dt\right]}{2\pi K T_0 B} \qquad \text{(A1)}$$

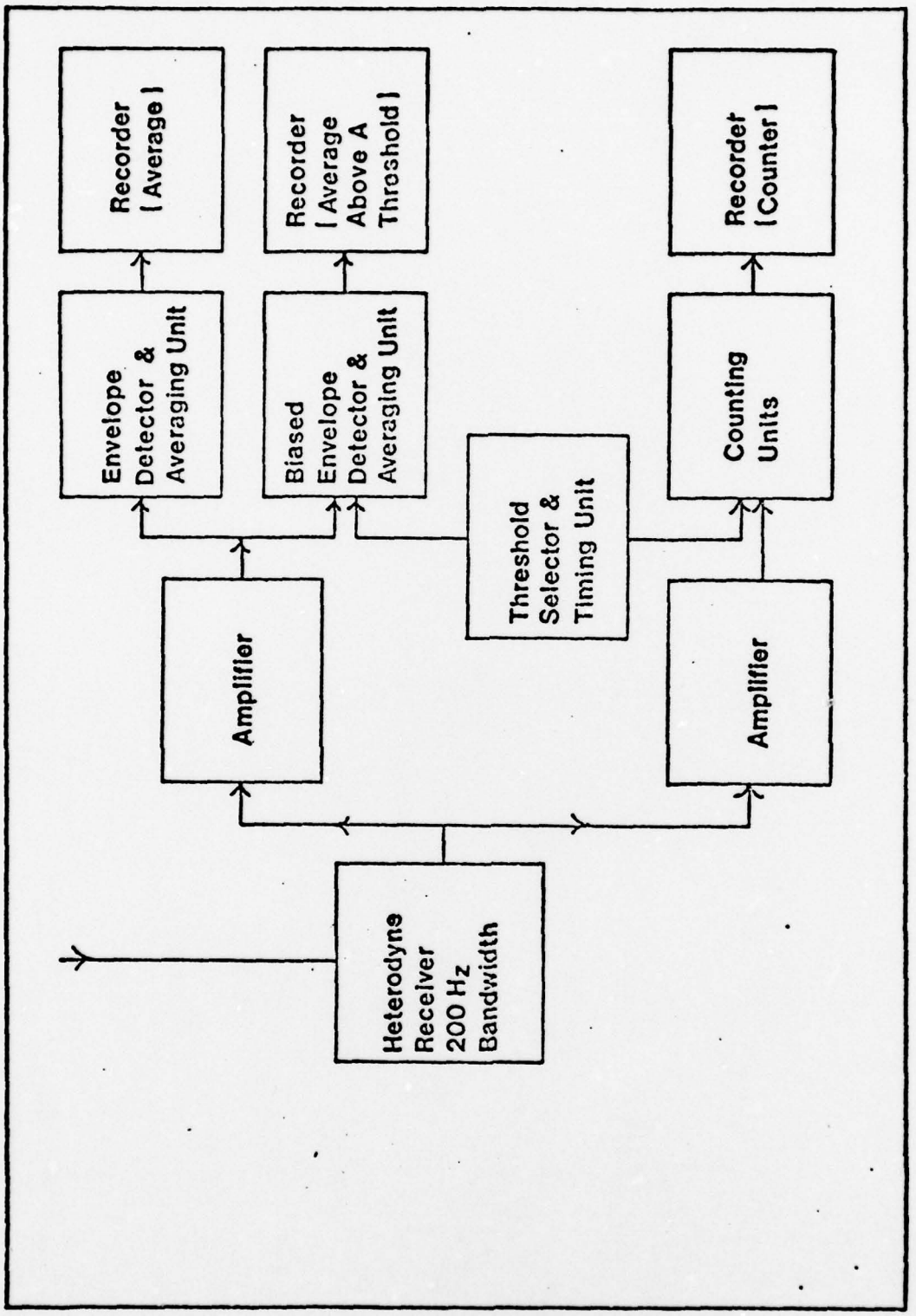

Fig. A1. Block Diagram of Receiver for Measuring ARM

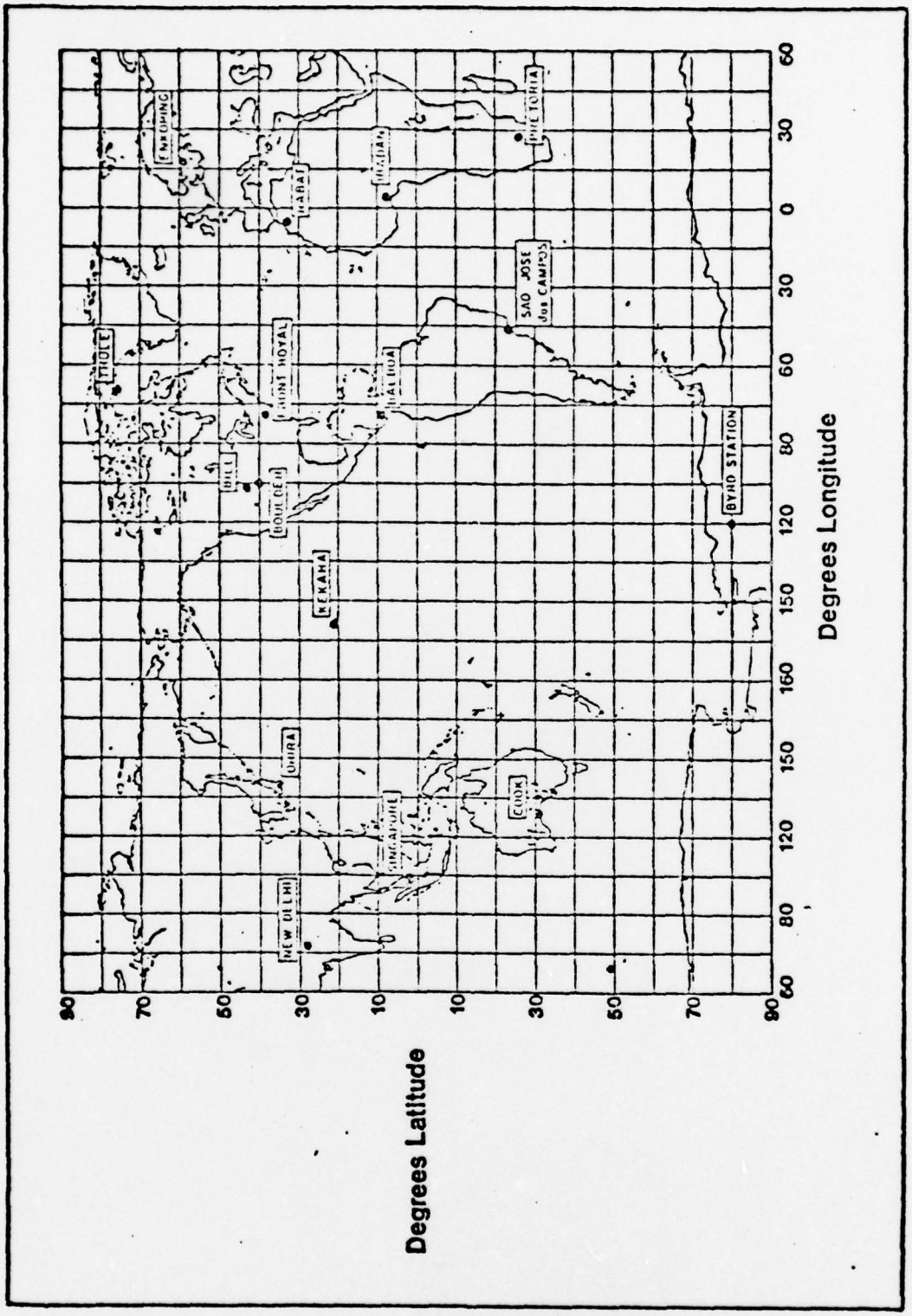

Fig. A2. Location of Receiving Stations Used to Compile Data for CCIR Report 322

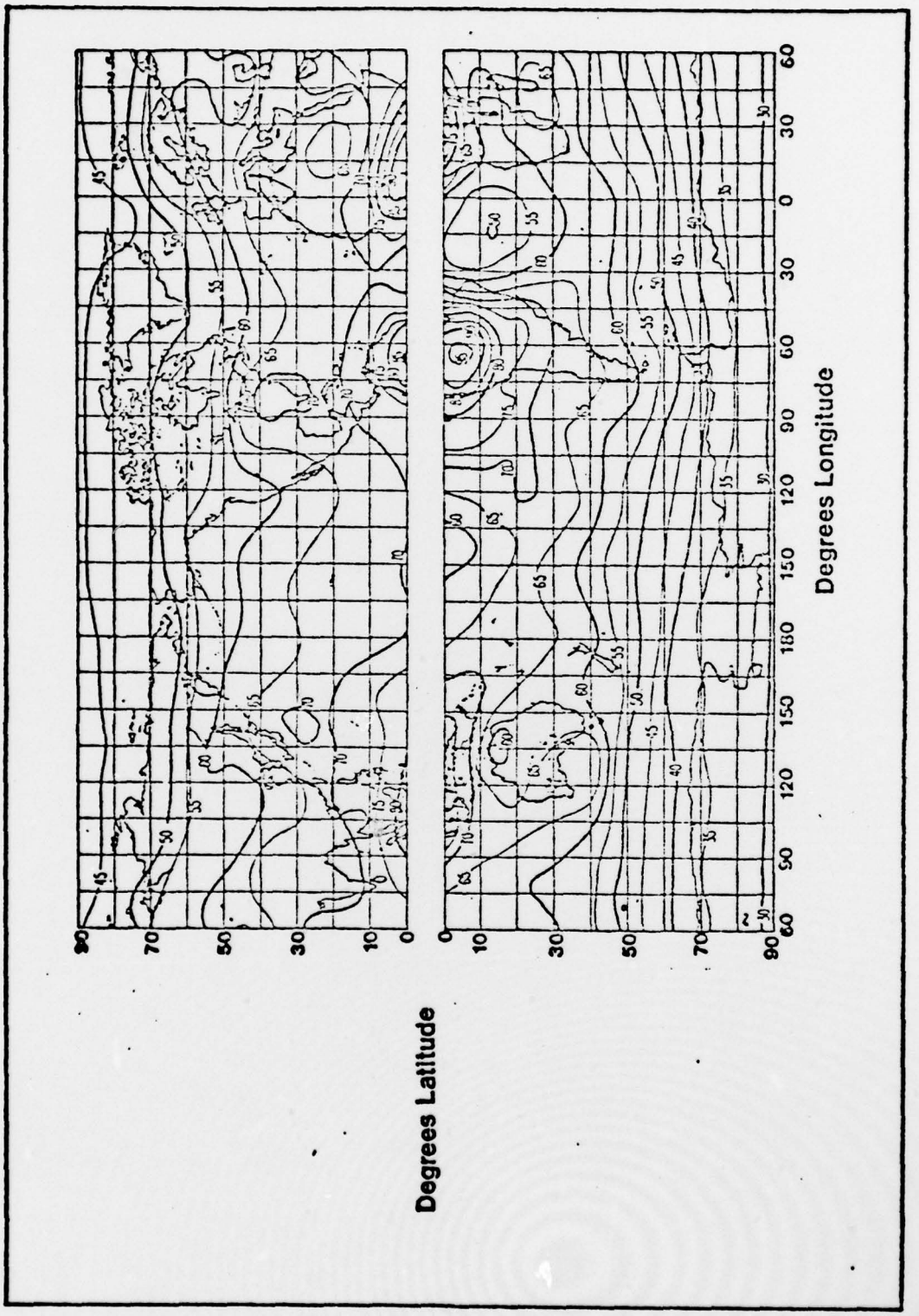

Fig. A3. A Typical Plot of Worldwide Average Noise Power as in CCIR Report 322

where

F_a = the average noise figure in db

K = Boltamn's constant

T_0 = Standard temperature of 280° Kelvin

E(t) = The time varying envelope waveform

T = The observation time in sec

B = the receiver bandwidth in Hertz

All of the noise power measurements in CCIR Report 322 are made by receivers with a 200 Hz effective bandwidth. Figure A4 shows an example of an empirically derived plot for converting the noise power measured at 1 MHz to the average noise power at a different frequency. A different noise power conversion plot is required for each worldwide plot of noise power.

CCIR Report 322 also contains a plot of the amplitude-probability distribution (APD) of the ARN. The APD curve is a plot showing the percenage of the time that the time varying envelope voltage, at the output of an envelope detector, exceeds some threshold. The curve is plotted parametrically with V_d, which is defined by Eqs (A2), (A3), and (A4). The V_d ratio is a rough measure of the impulsiveness of the noise; the more impulsive, the larger the V_d ratio.

$$E_{rms} = \left[\frac{1}{T}\int_0^T E^2(t)dt\right]^{\frac{1}{2}} \qquad \text{(A2)}$$

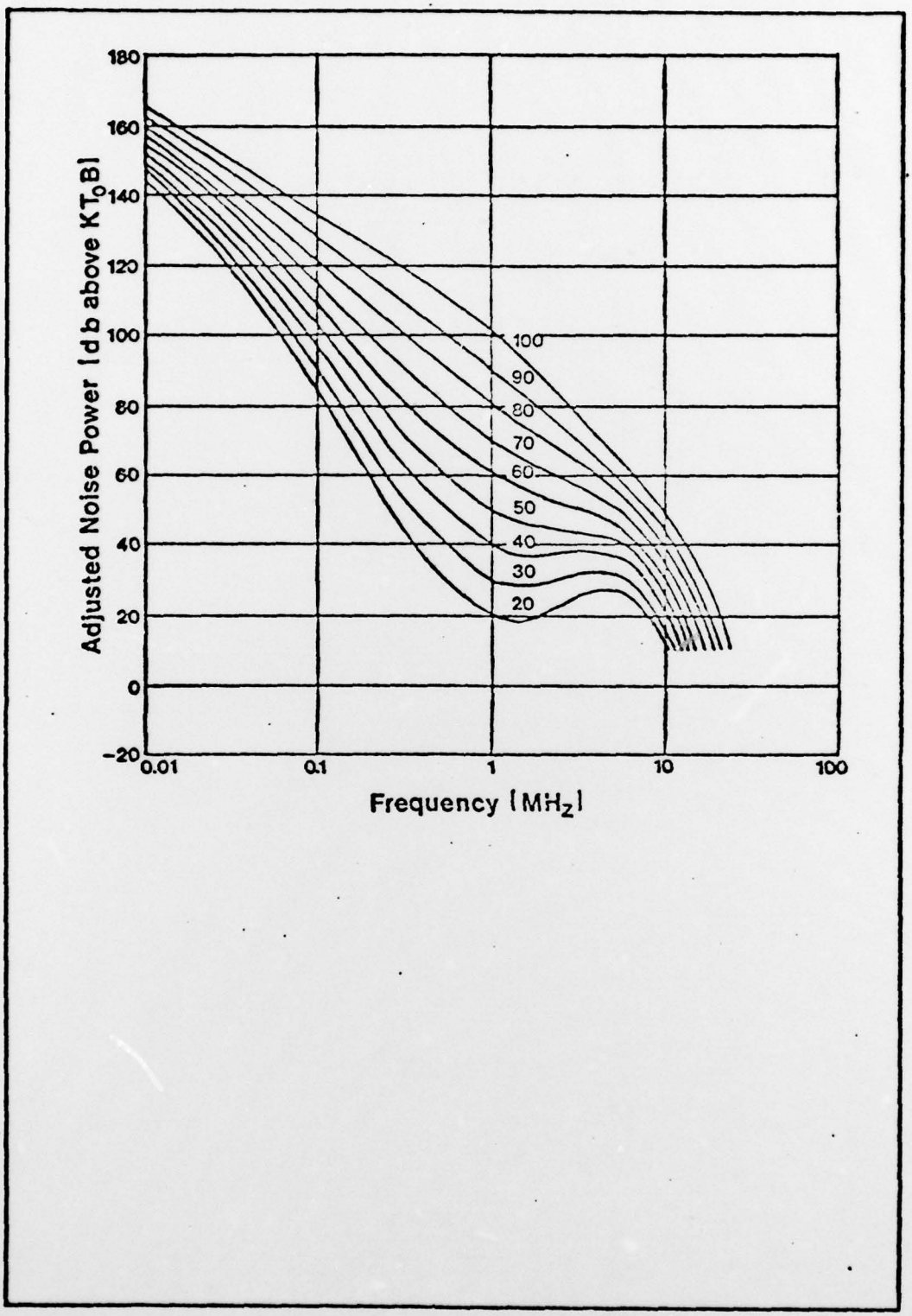

Fig. A4. Typical Noise Power Conversion Plot as in CCIR Report 322

$$E_{av} = [\frac{1}{T} \int_0^T E(t)dt] \tag{A3}$$

$$V_d = 20 \text{ LOG}_{10}\left(\frac{E_{rms}}{E_{av}}\right) \tag{A4}$$

The shapes of the APD curves depend only on the V_d ratio, rather than the absolute value of E_{rms} or E_{av} (Ref 1:1). Thus, all of the APD curves with a given V_d ratio can be collapsed into a sngle curve by normalizing the incoming waveform by E_{rms}, such that the resulting waveforms all have power equal to 1 watt (Ref 22:8-9). Since the waveforms have been normalized by E_{rms}, the envelope voltage threshold E_T must also be normalized. Therefore the ordinate of the APD plots is presented in terms of a threshold, Δ, which is defined in Eq (15).

$$\Delta = 20 \text{ LOG}_{10}\left(\frac{E_T}{E_{rms}}\right) \tag{A5}$$

where

E_T = envelope voltage threshold.

The APD plot shown in Figure A5 represents the amount of time the envelope waveform exceeds a threshold for a given V_d.

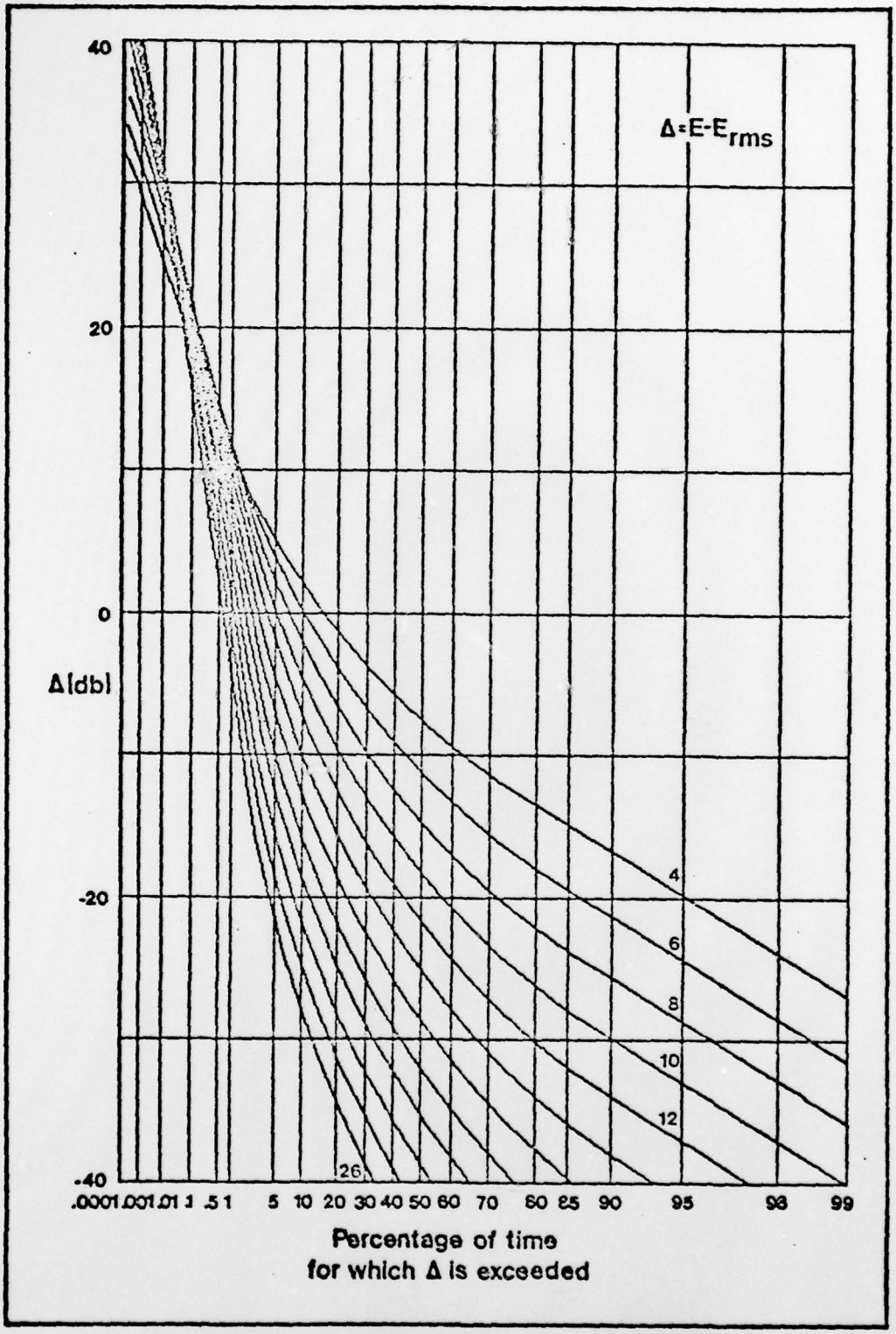

Fig. A5. Measured-Probability Distribution for ARN

Both the noise figure, F_a, and the APD curves are dependent on the receiver bandwidth (Ref 15). The receiver used by the National Bureau of Standards has an effective noise power bandwidth of 200 Hz. The APD curves in Figure A5 can be modified to apply to receivers of bandwidth other than 200 Hz. This can be done by selecting a curve with a different V_d. Figures A6 and A7 can be used to convert a V_d ratio measured by a receiver of one bandwidth to that of a different bandwidth (Ref 15).

The APD curves in CCIR Report 322 are composed from measurements made in different seasons of the year and times of the day. Due to the long-term variations that occur with time, the curves can only be considered an approximation to an APD curve that might be measured over any short period of time. Crichlow does not believe this introduces an appreciable error in computations using the APD curves (Ref 1:10).

All of the measurements made in CCIR Report 322 relate to the statistics of the time varying envelope waveform of the noise. If the envelope noise process is modeled as a stochastic process that is ergodic in both the mean, and autocorrelation, then the measurements of average noise power and the average envelope amplitude from CCIR Report 322 are representative of the second and first moments of the first order probability density function of the noise process. If the process is ergodic in the mean, then it is also ergodic in distribution (Ref 9:328-332). Therefore, the measured APD curves can be related to the first order cumulative distribution function of the envelope noise process. The assumption of ergodicity over at least four-hour periods of time is required to make the noise measurements

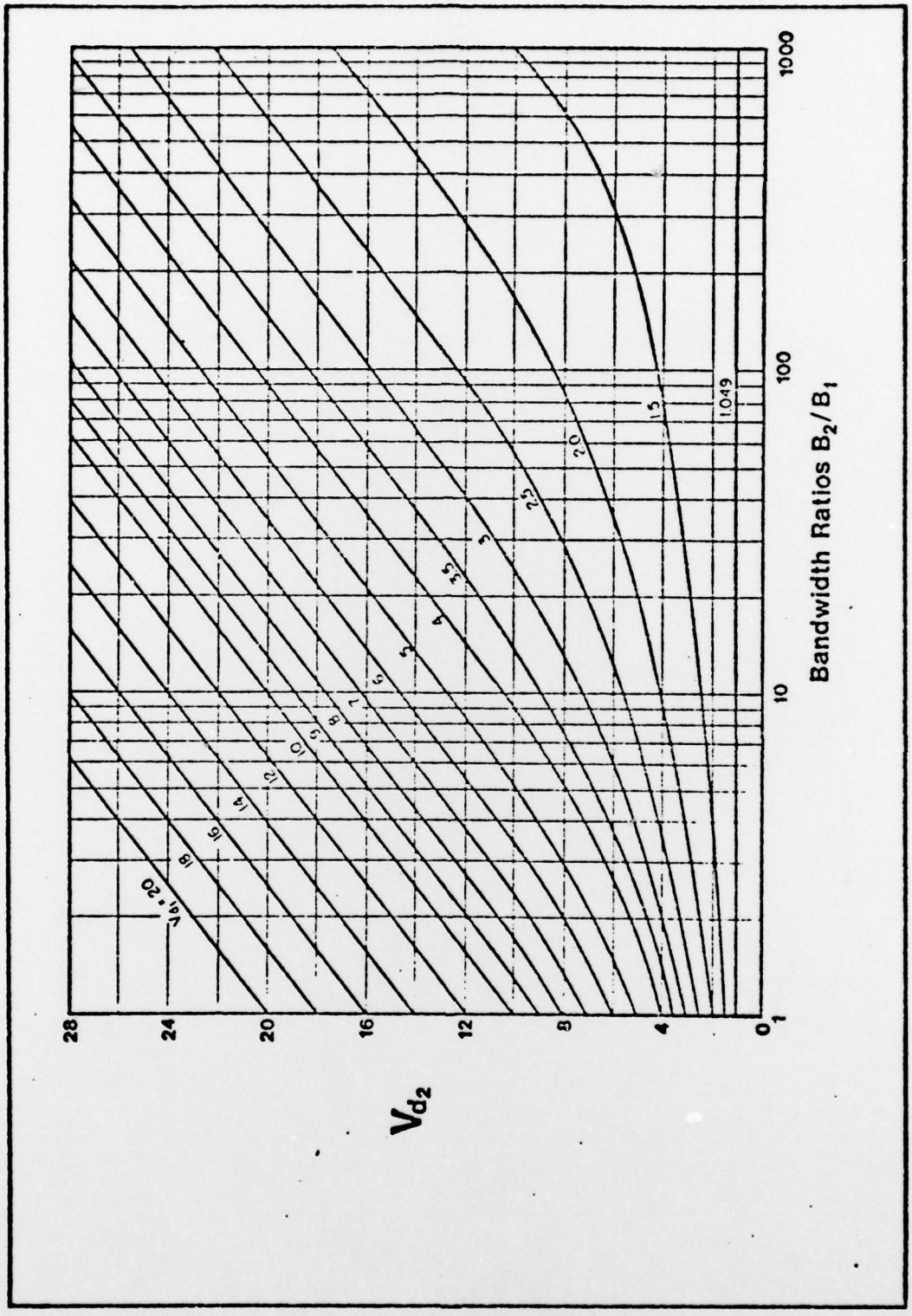

Fig. A6. APD Bandwidth Conversion Plot 1

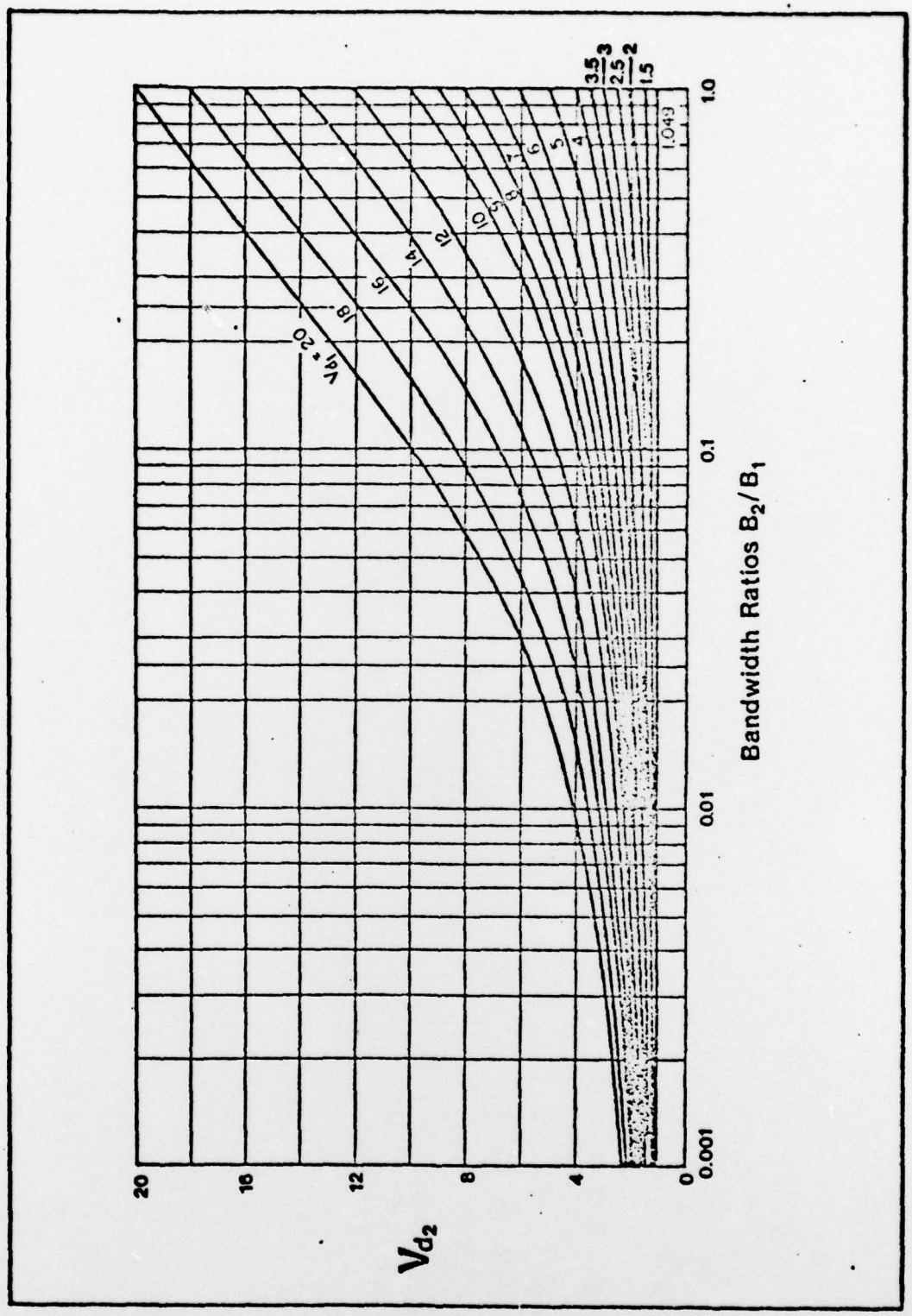

Fig A7. APD Bandwidth Conversion Plot 2

from CCIR Report 322 a meaningful measure of the statistical properties of the random process.

Appendix B: Numerical Integration of Equation 38

The purpose of this appendix is to discuss the numerical integration of $F_{\underset{\sim}{R}}(R_0)$ given at the end of Chapter IV. This equation is

$$F_{\underset{\sim}{R}}(R_0) = \exp\left[-T(\lambda_a+\lambda_b)\right. \cdot R_0 \int_0^{R_0} J_1(\rho R_0)\exp[T(\lambda_a I_0(Z_a)\exp(-Z_a) + \lambda_b I_0(Z_b)\exp(-Z_b)]\, d\rho \qquad \text{(B.1)}$$

where

$$Z_a = \frac{\rho^2\sigma_a^2}{4}$$

and

$$Z_b = \frac{\rho^2\sigma_b^2}{4}$$

The exponential form of $I_0(Z)$ given in Eq. (B.2) shows that for large ρ, the exponent will approach zero.

$$I_0(Z) \simeq \frac{e^Z}{\sqrt{2\pi Z}}\left(1+\frac{1}{8Z}\right) \qquad \text{(Ref 17)} \qquad \text{(B.2)}$$

for $Z \gg 1$.

It then follows that the exponential term approaches the value 1 and eventually has little effect on the integral as ρ gets large. Therefore, the integral is done in two sections.

The first section of theintegral was done using the trapezoidal rule. This section is ended when the exponent becomes less than a set threshold value. Since for small X, $\exp(X) \simeq 1+X$ so the threshold is directly related to the error in the approximation that $\exp(X)=1$. The threshold value used for the given curves was .0001 which allowed the integral to be evaluated in a reasonable amount of time. The bessel functions were evaluated using a routein supplied by the computer.

The final section is then

$$\int_{\rho_1}^{\infty} R_0 J_1(\rho R_0) d\rho$$

where ρ_1, is the last value of the first integration. By letting $u=\rho R_0$, $d\rho=du/R_0$ so that the integral is reduced to

$$\int_{\rho_1/R_0}^{\infty} J_1(u)du = J_0(\frac{\rho_1}{R_0})$$

Therefore, the integral can be defined as,

$$F_{\underset{\sim}{R}}(R_0) = \exp[-T(\lambda_a+\lambda_b)][R_0\Sigma_1+J_0(\frac{\rho_1}{R_0})] \qquad \text{(B.3)}$$

where Σ_1 is the integral to ρ_1.

VITA

John F. Stach was born September 20, 1956, in Detroit, Michigan. His family moved to Grand Blanc, Michigan in 1965 where he lived until graduation from high school. He then moved to Houghton, Michigan, where he attended Michigan Technological University. He was married in 1977 and graduated with honors in electrical engineering in 1978. He received a commission in the USAF upon graduation. He was then stationed at the Air Force Institute of Technology at Wright Patterson Air Force Base, Ohio.

Permanent address: 6203 Lake Forest Dr
Grand Blanc, Mich 48439

UNCLASSIFIED
SECURITY CLASSIFICATION OF THIS PAGE *(When Data Entered)*

REPORT DOCUMENTATION PAGE		READ INSTRUCTIONS BEFORE COMPLETING FORM
1. REPORT NUMBER AFIT/GE/EE/79-34	2. GOVT ACCESSION NO.	3. RECIPIENT'S CATALOG NUMBER
4. TITLE *(and Subtitle)* VALIDATION AND RECEIVER DESIGN FOR A RANDOM POINT PROCESS MODEL OF ATMOSPHERIC RADIO NOISE		5. TYPE OF REPORT & PERIOD COVERED MS Thesis 6. PERFORMING ORG. REPORT NUMBER
7. AUTHOR(s) John F. Stach 2nd Lt USAF		8. CONTRACT OR GRANT NUMBER(s)
9. PERFORMING ORGANIZATION NAME AND ADDRESS Air Force Institute of Technology (AFIT/EN) Wright-Patterson AFB, Ohio 45433		10. PROGRAM ELEMENT, PROJECT, TASK AREA & WORK UNIT NUMBERS
11. CONTROLLING OFFICE NAME AND ADDRESS Rome Air Development Center/DCCL Griffiss AFB NY 13441		12. REPORT DATE December 1979 13. NUMBER OF PAGES 64
14. MONITORING AGENCY NAME & ADDRESS*(if different from Controlling Office)*		15. SECURITY CLASS. *(of this report)* Unclassified 15a. DECLASSIFICATION/DOWNGRADING SCHEDULE

16. DISTRIBUTION STATEMENT *(of this Report)*

Approved for public release; distribution unlimited

17. DISTRIBUTION STATEMENT *(of the abstract entered in Block 20, if different from Report)*

18. SUPPLEMENTARY NOTES

Approved for public release; IAW AFR 190-17

JOSEPH P. HIPPS, Maj, USAF
Director of Public Affairs

19. KEY WORDS *(Continue on reverse side if necessary and identify by block number)*

ATMOSPHERIC RADIO NOISE
VERY LOW FREQUENCY
RANDOM PROCESSES
NOISE
POISSON PROCESSES
RECEIVER MODEL
OPTIMIZED RECEIVER

20. ABSTRACT *(Continue on reverse side if necessary and identify by block number)*

An investigation of low frequency atmospheric radio noise (ARN) indicates that the return stroke from lightning discharges is the major source of the noise. A model of ARN is then presented which is based on the return stroke. The model consists of the sum of two marked Poisson processes. The sum of marked Poisson processes can be thought of as a single marked Poisson process with a transformed rate and a mixture density on the marks. The complete statistical description of this process is then derived and a minimum probability of error processor is designed using the ARN model as

DD FORM 1 JAN 73 1473 EDITION OF 1 NOV 65 IS OBSOLETE

UNCLASSIFIED
SECURITY CLASSIFICATION OF THIS PAGE *(When Data Entered)*

the noise. The theoretical amplitude probability distribution (APD) is then derived for the output of a quadrature envelope detector using the ARN model as an input. The theoretical APD curves were then compared to a measured APD curve from CCIR Report 322 and two measured APD curves from an article by K. Furutsu and T. Ishida. The linear mean square error (MSE) between the theoretical and measured curves when plotted on Rayleigh paper is .018, and .015 for the Furutsu and Ishida data and .018 for the CCIR data. Based on the first order statistics, the model is found to be a good representation of low fre uency ARN. It is therefore recommended that the model be used to evaluate receiver performance in the low frequency channel and that a more thorough validation study be done including a validation of higher order statistics.